ORIGINAL PAPER

CrossMark

Optical properties of PVC/Al$_2$O$_3$ nanocomposite films

T. A. Taha[1] (ORCID)

Abstract

In this work, polyvinyl chloride (PVC) polymer films doped with 0, 2, 4, and 6 wt% Al$_2$O$_3$ nanoparticles with average size of 10 nm were prepared by solution casting route. Al$_2$O$_3$ nanoparticles are found to possess rhombohedral crystal structure, and PVC is partly crystallized as confirmed with XRD analysis. SEM images showed that Al$_2$O$_3$ nanoparticles are well distributed in the PVC film surface. The direct optical energy gap (E_{opt}) decreased from 5.05 to 3.60 eV and Urbach energy (E_U) increased with increasing Al$_2$O$_3$ concentration. The typical excitation energy for electronic transitions (E_0), the dispersion energy (E_d), refractive index, dipole strength (f), average oscillator wavelength (λ_0), oscillator strength parameter (S_0), optical conductivity, and both static and high-frequency dielectric constants are found to increase with increasing Al$_2$O$_3$ content. The third-order nonlinear optical susceptibility ($\chi^{(3)}$) and the nonlinear refractive index (n_2) were estimated. Also, the ratio of free carriers to effective mass (N/m^*) increased from 2.69×10^{57} to 170.91×10^{57} m^{-3} kg^{-1} with increasing Al$_2$O$_3$ nanoparticles percentage. Finally, the group velocity dispersion (GVD), dispersion coefficient for material dispersion (D), and third-order dispersion (TOD) are found to increase upon increasing Al$_2$O$_3$ filler ratio.

Keywords Polymer nanocomposite · PVC · Al$_2$O$_3$ nanoparticles · Optical conductivity · Dispersion parameters

Introduction

Polymer nanocomposites have induced a lot of interest in each academic and industrial application [1–7]. Polyvinyl chloride (PVC) polymer has been studied intensively because of its attention-grabbing physical properties [8–11]. The optical properties of those materials may be altered through the addition of various nanoparticle

✉ T. A. Taha
  taha.hemida@yahoo.com

1   Physics and Engineering Mathematics Department, Faculty of Electronic Engineering,
    Menoufia University, Menouf 32952, Egypt

ratios that could be used in optical fibers, optical waveguides and optical storage systems [1, 3, 6]. Optical properties of PVC compound films doped with numerous nanoparticles are investigated over the previous decades. Deshmukh et al. [12] considered the optical properties of PVC–PMMA thin films doped with 0.2, 0.4, 0.6, 0.8, and 1.0 wt% polyaniline (PANI). The optical energy gap (E_{opt}) increased with increasing PANI content except for the sample doped with 0.8 wt%, but the band-tailing decreased with increasing PANI concentration except for the samples doped with 0.6 and 1.0 wt%. The refractive index and high-frequency dielectric constant values indicated variety with PANI content. The ratio of free carriers to effective mass (N/m^*) values are found to be within the order of 10^{21} cm^{-3}/gm. Structure, optical and thermal properties of PVC/Cd$_{0.5}$Zn$_{0.5}$O nanocomposite films are explored [13]. The UV–Vis absorption spectra indicated that the prepared films are highly transparent and the transparency at higher slightly decreased with increasing Cd$_{0.5}$Zn$_{0.5}$O percentage from 0 to 0.5 wt% as a results of light scattering due to large aggregates. Optical properties of PVC-MWCNT nanocomposite films with totally different concentrations (0, 0.0005, 0.005, and 0.05 wt%) are contemplated [14]. The optical absorption increased with increasing MWCNT content. The direct optical energy gap decreased from 5.56 to 4.2 eV with increasing MWCNT percentage. The calculated refractive index, real and imaginary dielectric constants are found to increase with increasing MWCNT concentration. El Sayed and Morsi demonstrated that the direct band gaps and transparency of PVC/PbO nanocomposite films decreased with increasing PbO nanoparticles concentration [15]. The Urbach energies and refractive index of these nanocomposite films increased with increasing PbO nanoparticles content. Al-Taa'y et al. considered the impact of ZnO nanoparticles addition on the optical properties of polyvinyl chloride films [16]. The presence of ZnO causes an increase within the absorption and decrease within the nanocomposite films transparency. The extinction coefficient, refractive index, real and imaginary parts, optical conductivity, infinitely high-frequency dielectric constant, and average refractive index values increased with increasing ZnO content. The Urbach energy decreased with increasing ZnO concentration. The optical and dielectric properties of Cr$_2$O$_3$/PVC nanocomposite films have been explored [17]. The direct energy gap, single oscillator energy, and transparency decreased with increasing Cr$_2$O$_3$ concentration. However, Urbach energy, dispersion energy, refractive index at infinite wavelength, average interband oscillator wavelength, average oscillator strength, lattice dielectric constant and the ratio of carrier concentration to effective mass are found to increase with increasing Cr$_2$O$_3$ content. Structural, optical, and thermogravimetric analysis of Pb$_3$O$_4$/PVC nanocomposites films with totally different concentrations (0, 1, 2, 3, and 4 wt%) are contemplated [18]. The direct energy gap decreased from 5.05 to 4.34 eV with increasing Pb$_3$O$_4$ percentage. The presence of Pb$_3$O$_4$ nanoparticles enhanced the absorption and decreased the nanocomposite film transparency. Fermi energy, Urbach energy, and the solar material protection factor enhanced with increasing Pb$_3$O$_4$ wt%. This work aims to study the optical properties of PVC/Al$_2$O$_3$ nanocomposite films prepared by solution mixing and casting at room temperature. The linear optical parameters of these nanocomposites based on refractive index were calculated using Wemple–DiDomenico equation. The linear optical susceptibility ($\chi^{(1)}$), third-order nonlinear optical

susceptibility ($\chi^{(3)}$), and the nonlinear refractive index (n_2) were investigated. Also, the group velocity dispersion (GVD), dispersion coefficient for material dispersion (*D*), and third-order dispersion (TOD) are analyzed.

Experimental

In a common method, PVC/Al$_2$O$_3$ nanocomposite films with totally different concentrations (0, 2, 4, and 6 wt%) were prepared at room temperature. Two grams of PVC (extra pure powder with density 1.4 g/ml at 25 °C manufactured by Alpha Chemika, India) dissolved in 40 ml tetrahydrofuran (THF) and blended for 1 h on a magnetic stirrer, and then various ratios of Al$_2$O$_3$ nanoparticles are added to the clear solution with continuous stirring for one h. After that, the solution was thrown into glass Petri dish and left to dry in air to get the nanocomposite films.

XRD measurements of PVC/Al$_2$O$_3$ nanocomposite films were taken using XRD, Bruker, AXS D8 Advance, Germany, CuKa-radiation ($k = 1.542$). The size and morphology of Al$_2$O$_3$ nanoparticles were determined by transmission electron microscopy (TEM, JEOL 2100FX) worked at 200 kV accelerating voltage. Scanning electron microscopy (SEM) micrographs were recorded utilizing Quanta FEG250 SEM. The optical measurements of the synthesized PVC/Al$_2$O$_3$ nanocomposite films were taken utilizing JASCO UV–Vis–NIR double-beam spectrophotometer model V-570.

Results and discussion

Figure 1 shows XRD patterns of pure PVC and PVC + 4 wt% Al$_2$O$_3$ films; it is discovered that pure PVC is partly crystallized and also the diffraction peaks related to rhombohedral Al$_2$O$_3$ crystal [JCPDS card number 43-1484] with positions 25.50°, 37.68°, 43.07°, and 52.50° noticed for PVC film doped with 4 wt% Al$_2$O$_3$.

The average Al$_2$O$_3$ nanoparticles size determined from TEM micrograph (Fig. 2a) is 10 nm.

Scanning electron microscope (SEM) images are displayed in Fig. 2b–d that illustrated that Al$_2$O$_3$ nanoparticles are well distributed in PVC film surface.

The normalized optical absorption spectra for PVC compound films doped with 0, 2, 4, and 6 wt% Al$_2$O$_3$ nanoparticles are represented in Fig. 3. It is watched that the polymer films absorption increase with increasing Al$_2$O$_3$ nanoparticles content. The absorption band extended from 257 to 297 nm is appointed to π–π* electronic transition [18–20] and the increased absorbance at wavelengths below 257 nm is identified with C–Cl bond [18, 21].

The transmittance spectra and the first derivative of the optical transmittance for the nanocomposite films were plotted versus wavelength as shown in Fig. 4. The absorption band edges of those films were evaluated from the maximum peak position in Fig. 4b [22] and tabulated in Table 1. The addition of Al$_2$O$_3$ nanoparticles causes an increase in the maximum peak values from 269 to 316 nm as seen in Table 1. This leads to a decrease in the absorption band edge from 4.197 to 3.931 eV with the variation of Al$_2$O$_3$ percentage.
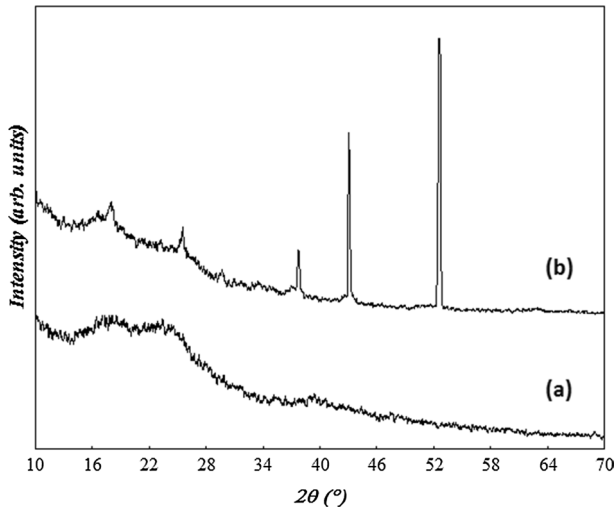
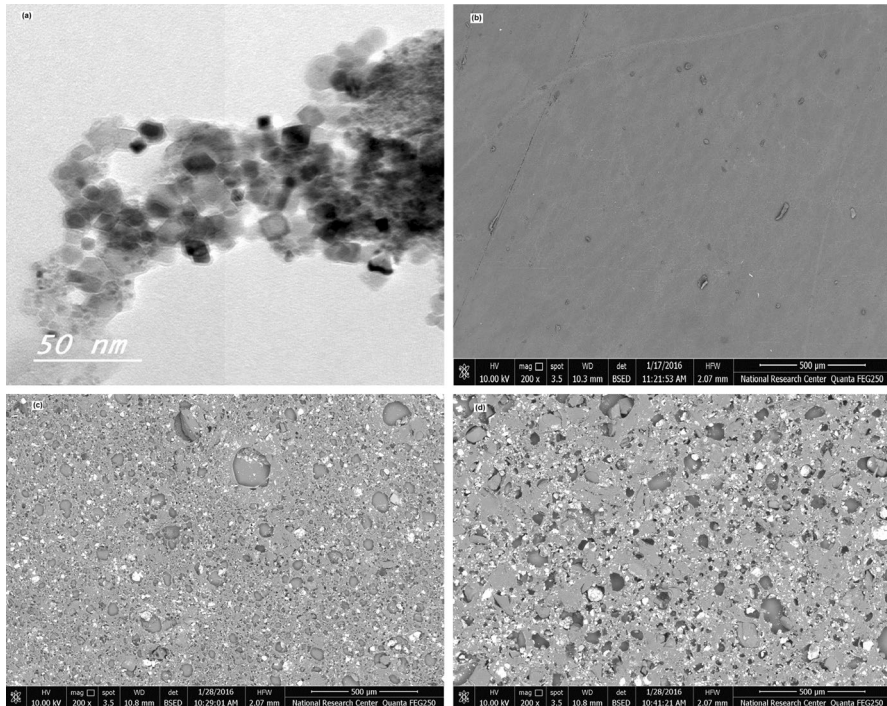**Fig. 1** XRD spectra of **a** pure PVC, **b** PVC doped with 4 wt% Al_2O_3

Fig. 2 **a** TEM micrograph of Al_2O_3 nanoparticles, **b** SEM image of pure PVC, **c** SEM image of PVC + 2 wt% Al_2O_3, **d** SEM image of PVC + 6 wt% Al_2O_3
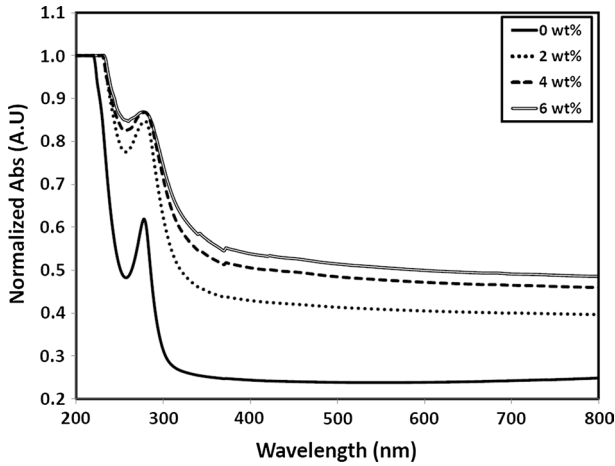
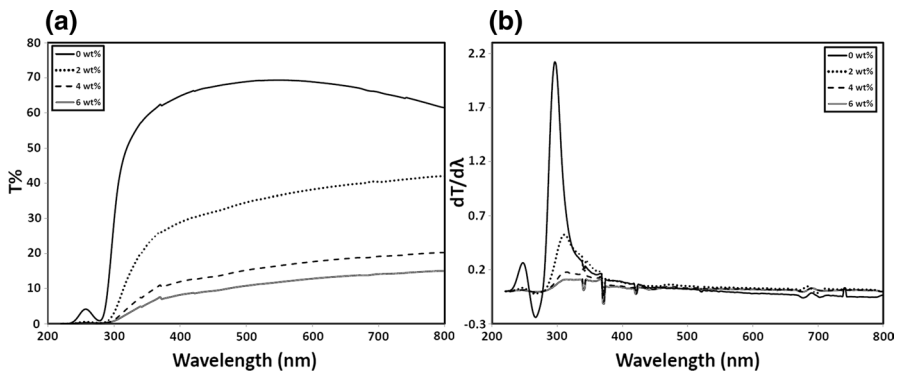**Fig. 3** Normalized optical absorption spectra for PVC/Al$_2$O$_3$ nanocomposite films

Fig. 4 a The transmittance versus wavelength plot and **b** the first derivative of the optical transmittance versus wavelength plot for the nanocomposite films

The optical band gap (E_{opt}) values for allowed direct transitions are calculated utilizing the well-known relation [23–25];

$$\alpha h\nu = k(h\nu - E_{opt})^{1/2} \tag{1}$$

where $h\nu$ is the incident photon energy and k is a constant. The direct band gaps, E_{opt}, are dictated by extrapolating the linear portion of the curves in Fig. 5a to zero absorption and summarized in Table 1. The addition of Al$_2$O$_3$ nanofiller results in localized states formation within the band gap and lowers the optical band gap values that are less than the band gap of pure PVC film [15, 18].

Table 1 Optical band gap (E_{opt}), Urbach energy (E_U) and other optical parameters for the PVC/Al$_2$O$_3$ nanocomposite films

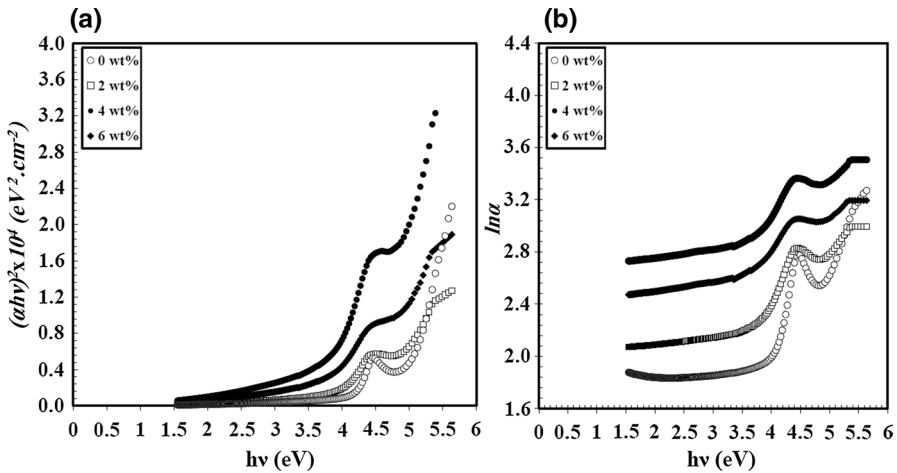| Samples	E_0 (eV)	E_d (eV)	f (eV)^2	n_0	ε_s	E_{opt} (eV)	E_U (eV)	λ_{max} (nm)	Absorption band edge (eV)	M_{-1}	M_{-3} (eV^{-2})
PVC+0 wt% Al$_2$O$_3$	5.05	7.14	36.06	1.55	2.41	5.05	0.78	296	4.197	1.414	0.055
PVC+2 wt% Al$_2$O$_3$	3.94	21.90	86.29	2.56	6.56	3.92	1.69	312	3.982	5.558	0.358
PVC+4 wt% Al$_2$O$_3$	3.87	76.01	294.16	4.54	20.64	3.70	2.21	316	3.932	19.641	1.311
PVC+6 wt% Al$_2$O$_3$	3.81	114.09	434.68	5.56	30.94	3.60	2.48	314	3.957	29.945	2.062

Fig. 5 **a** Plots of $(\alpha h\nu)^2$ versus $h\nu$ for the PVC/Al$_2$O$_3$ nanocomposite films, **b** variation of Lnα with photon energy ($h\nu$) for the prepared nanocomposite films

The width of band tails (E_U) for localized states within the forbidden band gap that is connected with the amorphous nature of the materials can be calculated via Urbach equation [26];

$$\ln(\alpha) = \ln(\alpha_0) + h\nu/E_U \tag{2}$$

where α_0 is a constant. E_U values were calculated from the inverse slope for straight lines of every curve in Fig. 5b.

The obtained values are found to increase with increasing Al$_2$O$_3$ wt% (Table 1), possibly due to the formation of imperfections and increased disorder within the nanocomposite [27, 28]. Likewise, it is seen that E_U values for PVC polymer films doped with 2, 4, and 6 wt% Al$_2$O$_3$ nanoparticles are higher than that for pure PVC film [18].

The refractive index, n, was computed using values of reflectance calculated from [29, 30];

$$R = 1 - \sqrt{T * \exp(A)} \tag{3}$$

Through the subsequent equation [25, 31];

$$n = \left(\frac{1+R}{1-R}\right) + \left(\frac{4R}{(1-R)^2} - k^2\right)^{\frac{1}{2}} \tag{4}$$

where k is the extinction coefficient ($k = \alpha\lambda/4\pi$). The dependence of refractive index on wavelength is represented in Fig. 6.

From investigation of this figure, it is ascertained that the refractive index for the current polymer nanocomposite films increases with increasing Al$_2$O$_3$ nanoparticles content and higher than that of pure PVC film. Also, the obtained refractive index
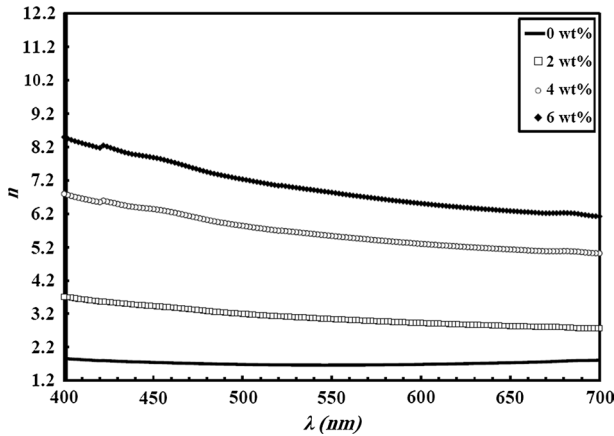
Fig. 6 Calculated refractive index as a function of wavelength for the PVC/Al$_2$O$_3$ films

values are higher than that in the literature [6, 14–16]. The increase in the refractive index values of these nanocomposite films may be due to the condensation of smaller ceramic molecules into larger clusters [32]. The high values of refractive index (typically > 1.65) for the PVC/Al$_2$O$_3$ nanocomposite films make it suitable in improving the performance of optical and photovoltaic devices in many technologies like solar cells [32, 33], Bragg gratings [34], photonic crystals [35] and waveguide-based optical circuits [36].

The refractive index dispersion of the prepared PVC/Al$_2$O$_3$ films is expressed by the formula [37];

$$\left(n^2 - 1\right)^{-1} = \frac{E_0}{E_d} - \left(\frac{1}{E_0 E_d}\right)(h\nu)^2 \tag{5}$$

where n is that the refractive index, $h\nu$ is the incident photon energy, E_0 is that the average excitation energy for electronic transitions and E_d is the dispersion energy that measure the interband optical transitions strength and is identified with the changes within the material structural order and also the effective oscillator energy. E_0 and i_d values were calculated from the slope and intercept on the vertical axis of $(n^2 - 1)^{-1}$ versus $(h\nu)^2$ plots (Fig. 7) and displayed in Table 1.

The static refractive index n_0 (at zero photon energy) is calculated by extrapolating Eq. 4 to $h \rightarrow 0$, that is obtained from the subsequent relation [37]:

$$n_0 = \sqrt{\left(1 + \frac{E_d}{E_0}\right)} \tag{6}$$

The static dielectric constant is computed from the static refractive index using $\varepsilon_s = n_0^2$ [38, 39] and also optical oscillator strengths (f) for optical transitions are defined as absorption of a photon by the electron between the initial state and the
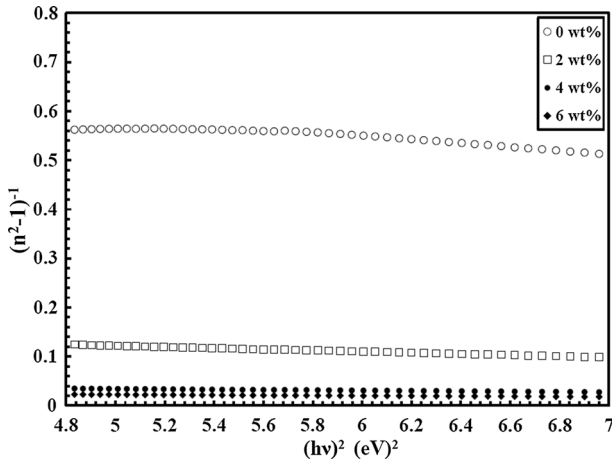
Fig. 7 $(n^2 - 1)^{-1}$ versus $(hv)^2$ plots for the PVC/Al$_2$O$_3$ films

final state that is correlated with E_0 and E_d as $f = E_0 E_d$ [30, 40]. The got values of n_0, ε_s and f are recorded in Table 1 which increased with increasing Al$_2$O$_3$ wt%.

The moments of optical spectrum M_{-1} and M_{-3} for the PVC/Al$_2$O$_3$ films were computed from the following relations [41];

$$E_0^2 = \frac{M_{-1}}{M_{-3}} \text{ and } E_d^2 = \frac{M_{-1}^3}{M_{-3}} \tag{7}$$

The M_{-1} and M_{-3} moments for the PVC/Al$_2$O$_3$ films were obtained and are found to increase with the addition of Al$_2$O$_3$ nanoparticles in Table 1.

The linear optical susceptibility $\chi^{(1)}$ for PVC/Al$_2$O$_3$ nanocomposite films could be computed from the relation [42, 43];

$$\chi^{(1)} = E_d/4\pi E_0 \tag{8}$$

The calculated $\chi^{(1)}$ values are given in Table 2 which are found to increase with increasing Al$_2$O$_3$ content. Additionally, the third-order nonlinear optical susceptibility $\chi^{(3)}$ is estimated utilizing the following formula [42, 44];

$$\chi^{(3)} = 6.82 \times 10^{-15} \left(E_d/E_0\right)^4 \quad \text{(e.s.u)} \tag{9}$$

The nonlinear refractive index for the prepared PVC/Al$_2$O$_3$ nanocomposite films may be written as [45–47]:

$$n_2 = \frac{12\pi\chi^{(3)}}{n_0} \tag{10}$$

Table 2 Values of S_0, λ_0, N/m^*, ω_p, n_∞, ε_∞, $\chi^{(1)}$, $\chi^{(3)}$, n_2 and for the PVC/Al$_2$O$_3$ nanocomposites

Samples	S_0 (m^{-2}) $*$ 10^{13}	λ_0 (nm)	N/m^* (m^{-3} kg^{-1}) × 10^{57}	ω_p (Hz) × 10^{15}	n_∞	ε_∞	$\chi^{(1)}$	$\chi^{(3)}$ × 10^{-12} (e.s.u)	n_2 ×10^{-10} (e.s.u)
PVC+0 wt% Al$_2$O$_3$	2.35	245.38	2.69	2.79	1.85	3.43	0.11	0.027	0.0066
PVC+2 wt% Al$_2$O$_3$	5.62	314.73	28.27	9.04	4.02	16.18	0.44	6.51	0.9586
PVC+4 wt% Al$_2$O$_3$	19.23	319.63	106.13	17.52	7.52	56.53	1.56	1014.9	84.2749
PVC+6 wt% Al$_2$O$_3$	28.57	323.71	170.91	22.23	9.40	88.40	2.38	5483.71	371.8183

The obtained $\chi^{(3)}$ and n_2 values are increased with increasing Al_2O_3 concentration (see Table 2).

The average oscillator wavelength λ_0 and oscillator strength S_0 parameter values for the considered nanocomposite samples can be acquired from the linear of $(n^2 - 1)^{-1}$ versus λ^{-2} (Fig. 8) by utilizing the single oscillator demonstrate as [39];

$$\left(n^2 - 1\right)^{-1} = \left(\frac{1}{S_0\lambda_0^2}\right) - \left(\frac{1}{S_0}\right)\lambda^{-2} \tag{11}$$

The obtained λ_0 and S_0 values are given in Table 2. It is clear that the average oscillator wavelength λ_0 and oscillator strength S_0 parameter values increased with the steady increase in Al_2O_3 nanoparticles wt%.

The real part of the dielectric constant ε_1 can be analyzed to obtain the high-frequency dielectric constant ε_∞ as indicated by the following relation [48–51];

$$\varepsilon_1 = n^2 - k^2 = \varepsilon_\infty - \left(\frac{e^2}{4\pi^2c^2\varepsilon_0}\right)\left(\frac{N}{m^*}\right)\lambda^2 \tag{12}$$

where λ is the wavelength, e is that the charge of the electron, N is that the free charge-carrier concentration, ε_0 is the permittivity of the free space, m^* the effective mass of the charge carriers (kg), and c is that the velocity of light in vacuum. The high-frequency dielectric constant ε_∞ and (N/m^*) can be calculated from the intercept and the slope of the linear portion in ε_1 versus λ^2 plots as appeared in Fig. 9. Moreover, the long wavelength refractive index n_∞, is calculated utilizing $\varepsilon_\infty = n_\infty^2$ and furthermore the plasma frequency ω_p is calculated from the relation; $\omega_p^2 = \frac{e^2N/m^*}{\varepsilon_0}$
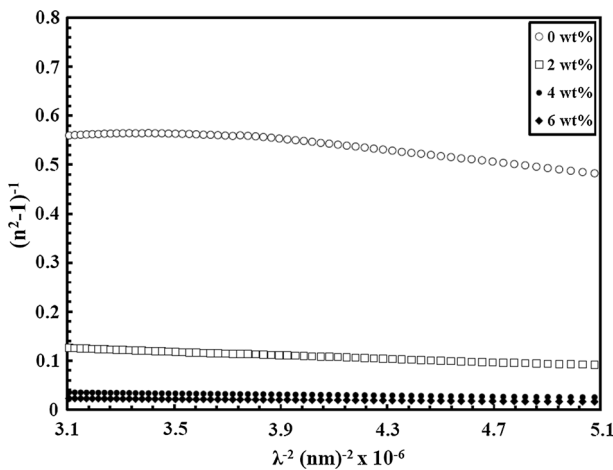
.

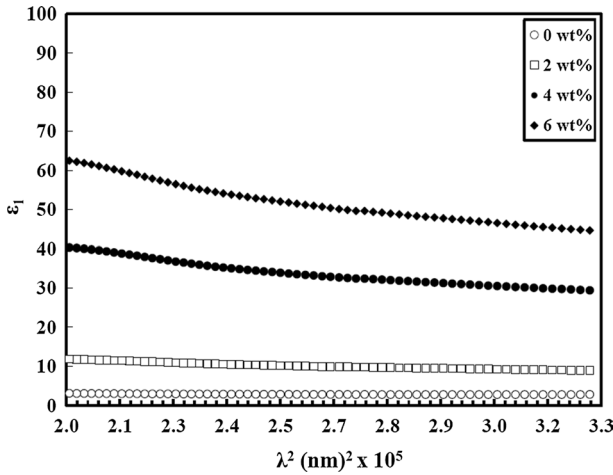**Fig. 8** $(n^2 - 1)^{-1}$ versus $(\lambda)^{-2}$ plots for the PVC/Al_2O_3 nanocomposite films

Fig. 9 Plots of ε_1 versus λ^2 for the prepared PVC/Al$_2$O$_3$ nanocomposite films

It is clear that the ratio of free carriers to effective mass (N/m^*) increase with increasing Al$_2$O$_3$ nanoparticles content as indicated in Table 2. Likewise, the plasma frequency (ω_p), n_∞, and ε_∞ are increased with increasing Al$_2$O$_3$ nanoparticles wt% for the prepared PVC/Al$_2$O$_3$ nanocomposite films.

The optical conductivity (σ_{opt}) comes because of the movement of the charge carriers by alternating electric field of the incident electromagnetic waves which is given by the equation below [52];

$$\sigma_{\text{opt}} = \frac{nc\alpha}{4\pi} \tag{13}$$

where n is that the refractive index, c is that the speed of light in vacuum, and α is the absorption coefficient. The calculated optical conductivity as a function of incident photon energy is displayed in Fig. 10.

The ascertained increase in polymer nanocomposite films optical conductivity with increasing Al$_2$O$_3$ nanoparticles content could also be a direct result of the formation of new levels within the band gap that facilitate crossing of the electrons from the valence band to those local levels to the conduction band, consequently the band gap decreases and also the conductivity increase [53].

Dispersion in PVC/Al$_2$O$_3$ nanocomposite films is defined by the group velocity dispersion (GVD) which is related to the second derivative of refractive index with respect to the incident light wavelength by [54];

$$\text{GVD} = \frac{\lambda^3}{2\pi c^2}\left(\frac{d^2 n}{d\lambda^2}\right) \tag{14}$$

GVD obtained values using second derivative of refractive index with respect to wavelength data plotted in Fig. 11 are given in Table 3, which causes a short pulse
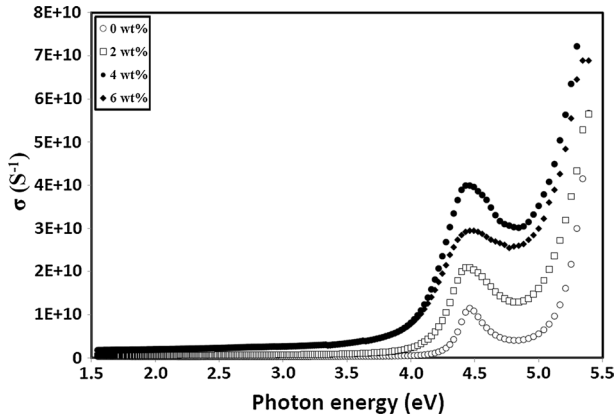
Fig. 10 The dependence of optical conductivity on the incident photon energy for the PVC/Al$_2$O$_3$ nanocomposite films
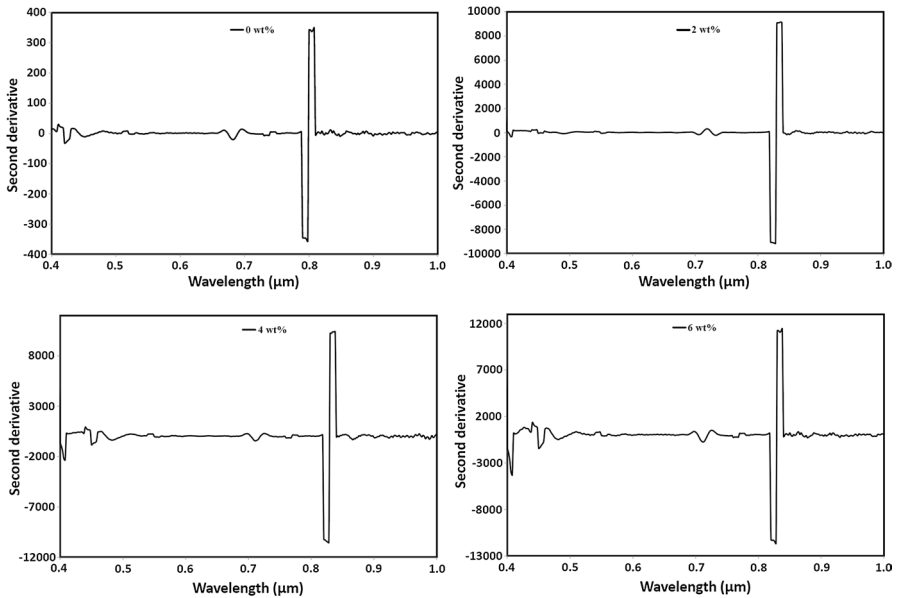

Fig. 11 Second derivative of refractive index with respect to wavelength for the PVC/Al$_2$O$_3$ nanocomposite films

Table 3 GVD, D, and TOD values for the PVC/Al$_2$O$_3$ nanocomposite films

Samples	GVD (fs^2/μm)	D (fs^2/μm^2)	TOD (fs^3/μm)
PVC+0 wt% Al$_2$O$_3$	326.05	−941.39	10331.05
PVC+2 wt% Al$_2$O$_3$	9477.56	−294965005.4	343929.02
PVC+4 wt% Al$_2$O$_3$	10821.32	−334.66	389961.03
PVC+6 wt% Al$_2$O$_3$	11909.10	−0.00725	407771.46

of light to spread in time as a result of different frequency components of the pulse traveling at different velocities. The dispersion coefficient for material dispersion (*D*) is related to GVD by [55];

$$D = -\frac{\lambda}{c}\left(\frac{d^2n}{d\lambda^2}\right) = -\frac{2\pi c}{\lambda^2}\text{GVD} \qquad (15)$$

The medium has positive dispersion, if *D* is less than zero. If *D* is greater than zero, the medium has negative dispersion. The third-order dispersion (TOD) is defined as the frequency dependence on GVD which is given by the following formula [54];

$$\text{TOD} = -\left(\frac{3\lambda^4}{4\pi c^3}\frac{d^2n}{d\lambda^2} + \frac{\lambda^5}{4\pi c^3}\frac{d^3n}{d\lambda^3}\right) \qquad (16)$$

The prepared polymer nanocomposite samples have high GVD as well as TOD, which increased with increasing Al_2O_3 nanoparticles concentration as seen in Table 3. Also, these samples have positive dispersion, as *D* values are less than zero.

Conclusion

PVC/Al_2O_3 nanocomposite films have been prepared successfully with the well-known solution casting route at room temperature. The optical parameters such as optical energy gap, Urbach energy, refractive index, dielectric constant, average oscillator wavelength, oscillator strength, bond strength, and optical conductivity were contemplated as a function of Al_2O_3 content and increase with increasing Al_2O_3. The third-order nonlinear optical susceptibility ($\chi^{(3)}$) and the nonlinear refractive index (n_2) are found to increase with increasing Al_2O_3 percentage that makes these films accommodating in optical devices technology. The group velocity dispersion, dispersion coefficient for material dispersion, and third-order dispersion were calculated and are found to increase with increasing Al_2O_3 percentage, which makes these films useful in laser pulse broadening.

References

1. Trindade T, Neves MC, Barros AMV (2000) Preparation and optical properties of CdSe/polymer nanocomposites. Scr Mater 43(6):567–571
2. Bhiwankar NN, Weiss RA (2006) Melt intercalation/exfoliation of polystyrene–sodium-mont-morillonite nanocomposites using sulfonated polystyrene ionomer compatibilizers. Polymer 47(19):6684–6691
3. Bouropoulos N, Psarras GC, Moustakas N, Chrissanthopoulos A, Baskoutas S (2008) Optical and dielectric properties of ZnO-PVA nanocomposites. Phys Status Solidi (a) 205(8):2033–2037
4. Sterky K, Jacobsen H, Jakubowicz I, Yarahmadi N, Hjertberg T (2010) Influence of processing technique on morphology and mechanical properties of PVC nanocomposites. Eur Polymer J 46(6):1203–1209
5. Roy AS, Gupta S, Sindhu S, Parveen A, Ramamurthy PC (2013) Dielectric properties of novel PVA/ZnO hybrid nanocomposite films. Compos B Eng 47:314–319

6. Ebnalwaled AA, Thabet A (2016) Controlling the optical constants of PVC nanocomposite films for optoelectronic applications. Synth Met 220:374–383
7. Abdullah OG, Salman YA, Saleem SA (2016) Electrical conductivity and dielectric characteristics of in situ prepared PVA/HgS nanocomposite films. J Mater Sci Mater Electron 27(4):3591–3598
8. Al-Hartomy OA, Al-Salamy F, Al-Ghamdi AA, Abdel Fatah M, Dishovsky N, El-Tantawy F (2011) Influence of graphite nanosheets on the structure and properties of PVC-based nanocomposites. J Appl Polym Sci 120(6):3628–3634
9. Kemal I, Whittle A, Burford R, Vodenitcharova T, Hoffman M (2013) Toughening of unmodified polyvinylchloride through the addition of nanoparticulate calcium carbonate and titanate coupling agent. J Appl Polym Sci 127(3):2339–2353
10. Mathur V, Patidar D, Sharma K (2015) Effect of nano CdS dispersion on thermal conductivity of PS/PVC and PS/PMMA polymeric blend nanocomposites. Appl Nanosci 5(5):623–628
11. Kobayashi S, Mullen K (2015) Encyclopedia of Polymeric Nanomaterials. Springer, Heidelberg, p 1740
12. Deshmukh S, Burghate D, Shilaskar S, Chaudhari G, Deshmukh P (2008) Optical properties of polyaniline doped PVC-PMMA thin films. Indian J Pure Appl Phys 46(5):344–348
13. Mahmoud WE, Al-Ghamdi AA (2011) The influence of Cd (ZnO) on the structure, optical and thermal stabilities of polyvinyl chloride nanocomposites. Polym Compos 32(7):1143–1147
14. Abdullah ET, Hasan SM, Naje AN (2013) Optical properties of PVC-MWCNT nano composites. Indian J Pure Appl Phys 51:77–80
15. Sayed AM, Morsi WM (2013) Dielectric relaxation and optical properties of polyvinyl chloride/lead monoxide nanocomposites. Polym Compos 34(12):2031–2039
16. Abdul Nabi M, Yusop RM, Yousif E, Abdullah BM, Salimon J, Salih N, Zubairi SI (2014) Effect of nano ZnO on the optical properties of poly (vinyl chloride) films. Int J Polym Sci 2014:697809-1–697809-6
17. Hassen A, El-Sayed S, Morsi WM, El Sayed AM (2014) Preparation, dielectric and optical properties of Cr2O3/PVC Nanocomposite films. J Adv Phys 4:571–584
18. Taha TA (2017) Optical and thermogravimetric analysis of Pb3O4/PVC nanocomposites. J Mater Sci Mater Electron 28(16):12108–12114
19. Allen NS, Edge M, Rodriguez M, Liauw CM, Fontan E (2000) Aspects of the thermal oxidation of ethylene vinyl acetate copolymer. Polym Degrad Stab 68(3):363–371
20. Giuffrida S, Condorelli GG, Costanzo LL, Ventimiglia G, Di Mauro A, Fragalà IL (2008) In situ synthesis of photoluminescent films of PVC, doped with Ce 3+ion. J Photochem Photobiol A 195(2):215–222
21. Mortazavi SH, Ghoranneviss M, Faryadras S (2012) Effect of low pressure nitrogen DC plasma on optical properties of biaxial-oriented polypropylene (BOPP), poly methyl methacrylate (PMMA) and poly vinyl chloride (PVC) films. J Fusion Energy 31(3):211–215
22. Gündüz B (2013) Effects of molarity and solvents on the optical properties of the solutions of tris [4-(5-dicyanomethylidenemethyl-2-thienyl) phenyl] amine (TDCV-TPA) and structural properties of its film. Opt Mater 36(2):425–436
23. Mahmoud WE, Al-Ghamdi AA, Al-Agel F (2011) Synthesis and optical properties of poly (vinyl acetate)/bismuth oxide nanorods. Polym Adv Technol 22(12):2055–2061
24. Mahmoud WE, Shirbeeny W, Al-Ghamdi AA, Al-Heniti S (2012) Synthesis and characterization of CdxZn1−xO nanoparticles-doped aryl poly ether ether ketone for novel application potentials. J Appl Polym Sci 125(1):339–343
25. Taha TA, Rammah YS (2016) Optical characterization of new borate glass doped with titanium oxide. J Mater Sci Mater Electron 27(2):1384–1390
26. Urbach F (1953) The long-wavelength edge of photographic sensitivity and of the electronic absorption of solids. Phys Rev 92(5):1324
27. Raja V, Sarma AK, Rao VN (2003) Optical properties of pure and doped PMMA-CO-P4VPNO polymer films. Mater Lett 57(30):4678–4683
28. Tommalieh MJ, Zihlif AM (2010) Optical properties of polyimide/silica nanocomposite. Phys B 405(23):4750–4754
29. Yahia IS, Farag AAM, Cavas M, Yakuphanoglu F (2013) Effects of stabilizer ratio on the optical constants and optical dispersion parameters of ZnO nano-fiber thin films. Superlattices Microstruct 53:63–75
30. Güneri E, Kariper A (2012) Optical properties of amorphous CuS thin films deposited chemically at different pH values. J Alloy Compd 516:20–26

31. Göde F (2011) Annealing temperature effect on the structural, optical and electrical properties of ZnS thin films. Phys B 406(9):1653–1659
32. Oubaha M, Elmaghrum S, Copperwhite R, Corcoran B, McDonagh C, Gorin A (2012) Optical properties of high refractive index thin films processed at low-temperature. Opt Mater 34(8):1366–1370
33. Leguijt C, Lölgen P, Eikelboom JA, Weeber AW, Schuurmans FM, Sinke WC, Verhoef LA (1996) Low temperature surface passivation for silicon solar cells. Sol Energy Mater Sol Cells 40(4):297–345
34. Cusano A, Iadicicco A, Paladino D, Campopiano S, Cutolo A, Giordano M (2007) Micro-structured fiber Bragg gratings. Part II: towards advanced photonic devices. Opt Fiber Technol 13:291–301
35. Kohoutek T, Orava J, Sawada T, Fudouzi H (2011) Inverse opal photonic crystal of chalcogenide glass by solution processing. J Colloid Interface Sci 353(2):454–458
36. Ho WF, Uddin MA, Chan HP (2009) The stability of high refractive index polymer materials for high-density planar optical circuits. Polym Degrad Stab 94(2):158–161
37. Sakr GB, Yahia IS, Fadel M, Fouad SS, Romčević N (2010) Optical spectroscopy, optical conductivity, dielectric properties and new methods for determining the gap states of CuSe thin films. J Alloy Compd 507(2):557–562
38. Wemple SH, DiDomenico M Jr (1971) Behavior of the electronic dielectric constant in covalent and ionic materials. Phys Rev B 3(4):1338
39. Wemple SH (1973) Refractive-index behavior of amorphous semiconductors and glasses. Phys Rev B 7(8):3767
40. Wemple SH, DiDomenico M Jr (1969) Optical dispersion and the structure of solids. Phys Rev Lett 23(20):1156
41. Gündüz B (2015) Sensing and surface morphological properties of a poly [(9, 9-dioctylfluorenyl-2, 7-diyl)-co-bithiophene] liquid-crystalline polymer for optoelectronic applications. J Appl Polym Sci 132(11):41659-1–41659-8
42. Frumar M, Jedelský J, Frumarova B, Wagner T, Hrdlička M (2003) Optically and thermally induced changes of structure, linear and non-linear optical properties of chalcogenides thin films. J Non-Cryst Solids 326:399–404
43. Gündüz B (2015) Optical properties of poly [2-methoxy-5-(3′, 7′-dimethyloctyloxy)-1, 4-phenylenevinylene] light-emitting polymer solutions: effects of molarities and solvents. Polym Bull 72(12):3241–3267
44. Ticha H, Tichy L (2002) Semiempirical relation between non-linear susceptibility (refractive index), linear refractive index and optical gap and its application to amorphous chalcogenides. J Optoelectron Adv Mater 4(2):381–386
45. Adair R, Chase LL, Payne SA (1989) Nonlinear refractive index of optical crystals. Phys Rev B 39(5):3337
46. Zahran HY, Yahia IS, Alamri FH (2017) Nanostructured pyronin Y thin films as a new organic semiconductor: Linear/nonlinear optics, band gap and dielectric properties. Phys B Condens Matter 513(95–102):39
47. Yakuphanoglu F, Cukurovali A, Yilmaz I (2004) Determination and analysis of the dispersive optical constants of some organic thin films. Phys B Condens Matter 351(1):53–58
48. Fadel M, Fayek SA, Abou-Helal MO, Ibrahim MM, Shakra AM (2009) Structural and optical properties of SeGe and SeGeX (X = In, Sb and Bi) amorphous films. J Alloy Compd 485(1):604–609
49. Khan SA, Al-Hazmi FS, Al-Heniti S, Faidah AS, Al-Ghamdi AA (2010) Effect of cadmium addition on the optical constants of thermally evaporated amorphous Se–S–Cd thin films. Curr Appl Phys 10(1):145–152
50. El-Korashy A, El-Zahed H, Radwan M (2003) Optical studies of [N (CH 3) 4] 2 CoCl 4,[N (CH 3) 4] 2 MnCl 4 single crystals in the normal paraelectric phase. Phys B 334(1):75–81
51. Wakkad MM, Shokr EK, Mohamed SH (2000) Optical and calorimetric studies of Ge–Sb–Se glasses. J Non-Cryst Solids 265(1):157–166
52. Pankove JI (1975) Optical processes in semiconductors. Dover Publications Inc., New York, p 91
53. Mansour AF, Mansour SF, Abdo MA (2015) Improvement structural and optical properties of ZnO/PVA nanocomposites. IOSR J Appl Phys 7(2):60–69
54. Diels Jean Claude, Rudolph Wolfgang (2006) Ultrashort laser pulse phenomena: fundamentals, techniques, and applications on a femtosecond time scale. Academic Press, USA, p 32
55. Gan F (1995) Optical properties of fluoride glasses: a review. J Non-Cryst Solids 184:9–20